Matter

CellPress

Article

Confined Interfacial Monomicelle Assembly for Precisely Controlled Coating of Single-Layered Titania Mesopores

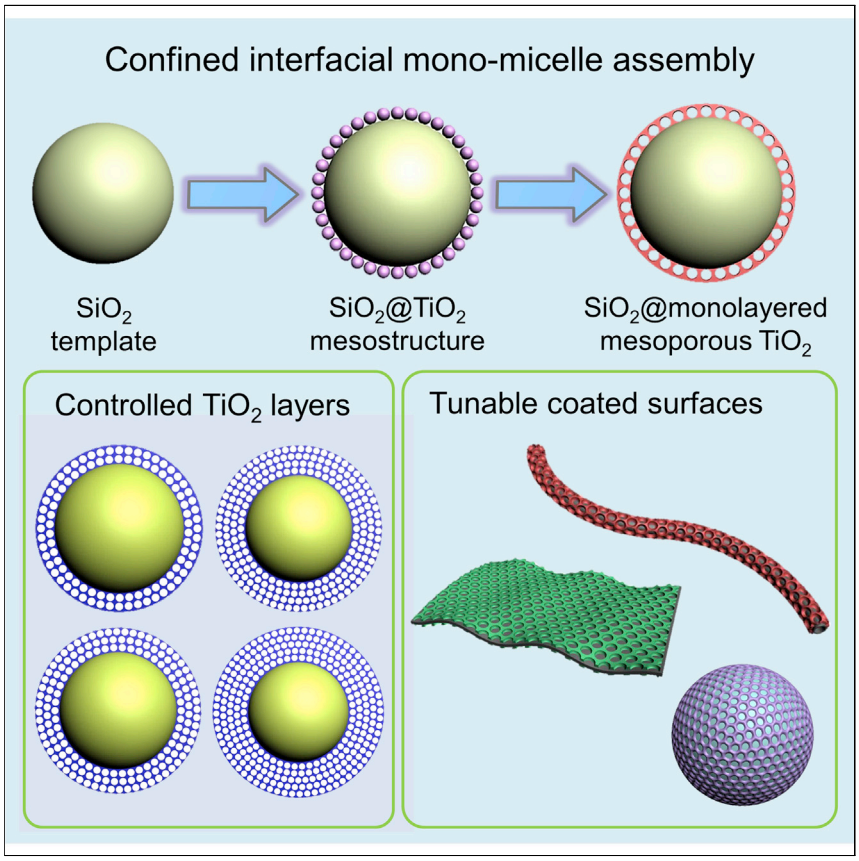

We have demonstrated a confined interfacial monomicelle assembly approach for accurately coating ordered monolayered TiO_2 mesopores on diverse surfaces. By regulating the synthetic conditions, the coated mesoporous TiO_2 layers can be well controlled with desired thickness, mesopore size, and switchable coated surfaces. The resulting monolayered mesoporous TiO_2 exhibit excellent sodium-storage properties. This unique mesoporous TiO_2 coating strategy affords great potential in constructing multicomponent nanostructures with mesoporosities for advanced technologies.

3 Understanding
Dependency and conditional studies on material behavior

Kun Lan, Yuan Xia, Ruicong Wang, ..., Xingmiao Zhang, Ahmed Elzatahry, Dongyuan Zhao

dyzhao@fudan.edu.cn

HIGHLIGHTS

A novel synthetic strategy was developed for coating single-layered TiO_2 mesopores

The assembly process showed great controllability and versatility

Extensive electrochemical sodium-storage properties were achieved

Lan et al., Matter 1, 527–538
August 7, 2019
https://doi.org/10.1016/j.matt.2019.03.003

Matter

CellPress

Article

Confined Interfacial Monomicelle Assembly for Precisely Controlled Coating of Single-Layered Titania Mesopores

Kun Lan,[1] Yuan Xia,[1] Ruicong Wang,[1] Zaiwang Zhao,[1] Wei Zhang,[1] Xingmiao Zhang,[1] Ahmed Elzatahry,[2] and Dongyuan Zhao[1,3,*]

SUMMARY

Mesoporous core-shell nanostructures have recently been receiving extensive scientific interest; however, reliable approaches for coating mesoporous materials still remain exciting challenges, except for amorphous silica. We report, for the first time, a confined interfacial monomicelle assembly method for controlled coating of anatase TiO_2 with single-layered ordered mesopores on diverse surfaces, opening up the area of coating ordered mesoporous crystalline materials that possess mesopores originating from self-assembled surfactant instead of accumulated nanocrystals. This facile and repeatable methodology relies on the solvent-confinement effect of glycerol during the assembly process and monomicelle hydrogel preformation by selective evaporation of double-solvent precursors. This assembly process shows precise controllability and great versatility, endowing the coated TiO_2 layers with highly tunable thickness, mesopore size, and switchable coated surfaces. The ultrathin monolayered mesopores of such mesoporous TiO_2 shells, in combination with their high surface area and highly crystalline nature, afford them excellent rate capability and superior cyclability for sodium-ion storage.

INTRODUCTION

Core-shell nanostructures have recently been receiving considerable scientific attention in various fields because of their combined functionalities of cores and shells, improved stabilities and dispersibilities of core particles, or even pristine photonic, electronic properties.[1–13] However, most shells formed around cores are commonly composed of dense or solid parts. Turning a dense shell into a mesoporous one provides markedly improved properties because such mesopores on shells are able to accommodate molecules and allow the diffusion into and out of cores due to their textural properties associated with the high pore volumes and surface areas.[14–16] A few advantageous examples include substantially enhanced reactant accessibilities and catalytic sites for mesoporous TiO_2 shells,[17,18] and much better conductivities and structural stabilities for mesocarbon-coated materials.[19]

The implementation of all these approaches strongly depends on constructing mesoporous-shelled nanostructures with controlled parameters, including composition, distribution, and thickness. A number of strategies have been developed to pursue these aims.[20–26] For instance, the representative surfactant-templating approach,[20] which involves soft core particles, structure-directing agents, and silica sources under alkaline conditions, has been widely used for coating various functional nanomaterials with mesoporous SiO_2 shells. Owing to its great simplicity and high

Progress and Potential

The development of core-shell structures has been in great demand recently owing to their integrated functionalities. However, the progress in reliable coating of porous semiconductors remains unproductive. Here, we have demonstrated a confined interfacial monomicelle assembly method for controlled coating of ordered single-layered mesoporous TiO_2. The coating method can be well controlled with tunable coated layers, mesopore size, and switchable coated surfaces. The resulting mesoporous TiO_2 exhibit excellent electrochemical properties as a sodium-ion anode, which is attributed to their unique mesostructures associated with accessible high surface area and ultrathin layers. Such accurately designed mesoporous core-shell nanostructures are expected to provide a useful platform to produce numerous delicate core-shell nanostructures with integrated functionalities and mesoporosities for potential applications, such as catalysts, sensors, energy storage, and energy conversion.

reproducibility, it can also be extended to fabricate SiO_2-based asymmetric nanoparticles[21] and yolk-shell nanostructures.[22,23] Unfortunately, these approaches cannot generate mesoporous core-shell structures with other compositions. The controllable coating of ordered mesoporous metal oxides, such as TiO_2 over functional cores, still remains an exciting challenge. Although TiO_2 has a sol-gel reaction quite similar to that of SiO_2, with similar molecular structures of precursors (e.g., tetrabutyl titanate [TBOT], tetraethyl orthosilicate), and both can form three-dimensional (3D) -O-M-O-M-O- networks,[27] the highly reactive titanium precursors endowed by the low electronegativity and high coordination number of titanium give rise to immense difficulties in precisely controlling the sol-gel chemistry of TiO_2 on interfaces.

As a consequence, the progresses in controlled coating of mesoporous TiO_2 shells remain underdeveloped. For instance, a general method similar to the Stöber process for silica has been developed to synthesize porous TiO_2 shells for constructing multifunctional core-shell particles,[28] but the mesopores normally generated from TiO_2 grain accumulation instead of surfactant-micelle templates are disordered and lack control. Alternatively, Guan et al. reported a method for coating mesoporous TiO_2 shells on various surfaces via a cooperative assembly-directed strategy.[29] However, such relatively small mesopores from hexadecylamine (HDA) and disordered structural regularity may hinder the efficient diffusion of guest molecules. Although other synthetic approaches such as utilizing "silica-protected calcination" to control TiO_2 grains[30] or the atomic layer deposition method[31,32] to deposit titania layers with ultrathin thickness (<1 nm) are able to successfully form nanoporous TiO_2 shells, the multistep processes are relatively tedious and the TiO_2 mesostructures cannot be highly adjusted. Precise control of the coating of mesoporous crystalline titania at the single-layer level has not been achieved to date. On the basis of these premises, the exploration of general and reliable synthetic methods for coating ordered mesoporous TiO_2 as a thin layer under delicate control is imperative.

We demonstrate a general confined interfacial monomicelle assembly approach to coat ordered single-layered crystalline TiO_2 mesopores in a precise, controllable manner. Here, we used coating colloidal SiO_2 nanospheres as a proof of concept. These highly ordered TiO_2 mesostructures controlled at single-micelle level can be heterogeneously assembled on diverse solid-liquid interfaces, which involves using triblock copolymer Pluronic F127 as a template and glycerol as a confined solvent. First, titania monomicelle hydrogels were prepared after preferential evaporation of tetrahydrofuran (THF). A sol-gel process was then initiated by subsequently mixing the monomicelles and solid silica cores into ethanol/glycerol solvents under stirring. We used high-viscosity glycerol as a co-solvent, because it enables induction of monomicellar self-assembly in spatially confined directions as well as simultaneously retarding hydrolysis and the condensation rate of titanium oligomers by strongly adhering to titania monomicelles.[33] As a result, the coated TiO_2 shells possess a monolayer of mesopores, a high surface area (119 $m^2\ g^{-1}$), and a large mean mesopore size (~9.8 nm), as well as crystalline anatase mesopore walls. Moreover, the accurate controllability of such a confined assembly process enables formation of TiO_2 shells from mono- to multilayers (up to five layers) of mesopores, and the mesopore size also can be manipulated from 4.7 to 18.4 nm by tuning the amount of swelling agent. We further show that the single-layered mesoporous TiO_2 shells can be grown on diverse functional nanomaterials, indicating their superior versatility. This novel type of single-layered mesoporous TiO_2-coated SiO_2 core-shell structure was denoted SiO_2@SL-mTiO_2, which exhibits superior

[1]Department of Chemistry, Shanghai Key Laboratory of Molecular Catalysis and Innovative Materials, Laboratory of Advanced Materials, iChEM (Collaborative Innovation Center of Chemistry for Energy Materials), Fudan University, Shanghai 200433, P.R. China

[2]Material Science and Technology Program, College of Arts and Science, Qatar University, Doha 2713, Qatar

[3]Lead Contact

*Correspondence: dyzhao@fudan.edu.cn

https://doi.org/10.1016/j.matt.2019.03.003

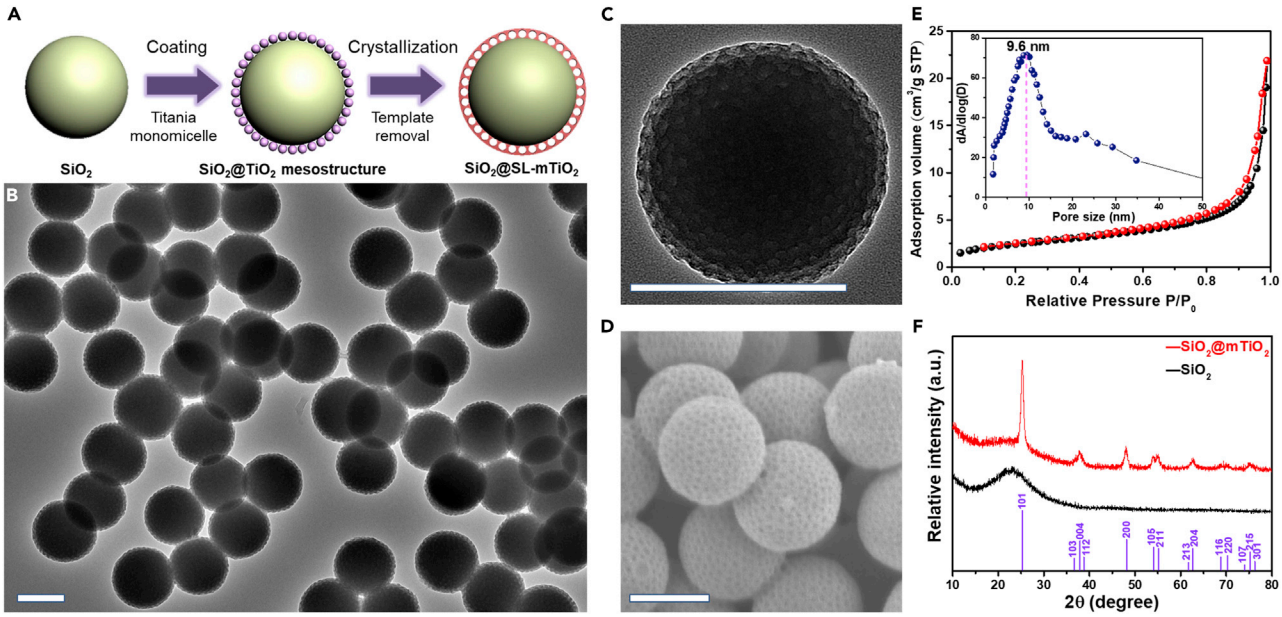

Figure 1. Synthesis and Characterization of the Single-Layered Mesoporous SiO_2@SL-mTiO_2 Core-Shell Nanostructures

(A) Schematic illustration of the preparation of single-layer TiO_2 mesopore-coated core-shell structures.

(B–D) Low-magnification TEM (B), high-magnification TEM (C), and FESEM (D) images of the SiO_2@SL-mTiO_2 core-shell nanostructures. Scale bars, 200 nm.

(E) Nitrogen-sorption isotherms and pore-size distribution of the SiO_2@SL-mTiO_2 core-shell nanostructures.

(F) WAXRD patterns of the SiO_2@SL-mTiO_2 and the pure silica nanospheres, compared to the standard anatase (space group $I4_1/amd$, JCPDS card No. 21–1272).

sodium-storage properties for sodium-ion batteries, including large discharge capacity, excellent rate capability, and outstanding cyclability.

RESULTS

Preparation and Characterization of the SiO_2@SL-mTiO_2 Nanostructures

Figure 1A presents the scheme for the coating of SL-mTiO_2, whereby the silica nanospheres with a diameter of about 220 nm (Figure S1) are used as a core substrate. The formed SiO_2@mTiO_2 core-shell hybrids possess an ultrathin mesoporous TiO_2 layer with a high uniformity (Figure 1B). The ordered open mesopores with a uniform mesopore size as large as ~9.5 nm are clearly evidenced from field-emission scanning electron microscopy (FESEM) images (Figure 1D). The magnified transmission electron microscopy (TEM) images show that the mesoporous TiO_2 shells are composed of closely packed open mesopores with a thickness of around 11.5 nm, indicating the formation of a single layer of closely packed uniform mesopores (Figures 1C and S2). Low-magnification FESEM images clearly reveal that every silica nanosphere is unexceptionally coated with a thin ordered TiO_2 mesostructure, and no homogeneous nucleation of TiO_2 monomicelles can be observed (Figure S3). Additionally the formed uniform SiO_2@SL-mTiO_2 nanospheres can further be packed into ordered photonic crystals by simple gravity sedimentation,[34] further confirming the substantial uniformity of the SiO_2@SL-mTiO_2 nanospheres and accuracy of the single-layered coating (Figure S4). The elemental mapping images (Figure S5) exhibit a homogeneous distribution of elements, including Ti, O, C, and Si, in whole core-shell nanospheres.

The zeta potential characterizations of the colloidal SiO_2 cores and SiO_2@SL-mTiO_2 hybrids further show a significant change from negative charge (−53.1 mV) to neutral (−0.54 mV) after coating SL-mTiO_2 layers (Figure S6), implying the success of TiO_2

growth entirely on the surface of silica cores. After removing the silica cores by NaOH etching treatment, the hollow SL-mTiO_2 spherical structures can be retained with a uniform thickness of around 9.7 nm (Figure S7). From nitrogen-sorption experiments (Figures 1E and S8A), both SiO_2@SL-mTiO_2 and hollow SL-mTiO_2 show type IV isotherms at a very high relative pressure P/P_0 = 0.6 to 1.0, indicating their uniform mesoporous structures, as also confirmed by the corresponding pore-size distribution curves (inset of Figures 1E and S8B). The Brunauer-Emmett-Teller surface area and mesopore volume of the hollow SL-mTiO_2 nanospheres are calculated to be as high as 119 $m^2\ g^{-1}$ and 0.28 $cm^3\ g^{-1}$, respectively. The wide-angle X-ray diffraction (WAXRD) patterns (Figure 1F) show a broad peak ranging from 15° to 30° for pure silica nanospheres. After the coating and annealing of TiO_2 layers, well-defined diffraction peaks at 25.4°, 37.0°, 48.1°, 54.2°, 55.0°, and 62.9° are observed, which can be indexed to the 101, 004, 200, 105, 211, and 204 reflections of anatase, fully confirming the formation of pure anatase phase (space group $I4_1/amd$) with a good crystallinity. The TiO_2 grain size calculated from Scherrer equation is about 5.1 nm, consistent with that (5.7 nm) observed from high-resolution TEM (HRTEM) results (Figure S9). The X-ray photoelectron spectra of the core-shell SiO_2@SL-mTiO_2 were further investigated and no peaks for Ti-C and Ti-Si bonding were detected (Figure S10), showing that the TiO_2 nanocrystals are connected with silica and carbon via an oxygen-linking bond or/and van der Waals force.

Precise Control of the Coated Mesoporous TiO_2 Layers

The structural parameters of the coated mesoporous TiO_2 layers can be highly controlled by regulating the synthetic conditions. A series of core-shell SiO_2@SL-mTiO_2 nanospheres with silica core diameters ranging from ~150 to 420 nm can be obtained by simply tuning the diameter of colloidal SiO_2 templates, demonstrating the general applicability of the confined monomicelle coating strategy (Figures 2A–2D and S11). More interestingly, if the glycerol amount decreases gradually from 10.0 to 3.0 mL, the numbers (one to five) of coated mesoporous TiO_2 layers can be accurately manipulated, and the resultant shell thickness varied from 11.5, 23.1, 32.5, 38.5 to 45.7 nm, respectively (Figures 2E–2N and S12). The mesoporous TiO_2 shells are estimated to possess near body-centered cubic mesostructures with *Im3m* symmetry according to small-angle X-ray scattering patterns, which requires further investigations due to the vague peaks of the distorted structures (Figure S12F). Also, the thickness exhibits a gradual increment from monolayer to five layers of mesopores with the increment of TBOT/SiO_2 weight ratio from 1:2.5 to 1:0.2 (Figure S13). From thermogravimetry curves, all the hollow mesoporous TiO_2 nanospheres show similar carbon weight ratio between 13.03% and 16.12% while the TiO_2 content exhibits a steady growth from 9.67% to 48.96% to SiO_2@SL-mTiO_2 when increasing mesoporous TiO_2 layers (Figure S14 and Table S1).

In addition to the tunable mesoporous TiO_2 layers, SiO_2@SL-mTiO_2 core-shell structures with controlled mesopore sizes can be easily prepared (Figures S15 and S16; Table S2). Without the addition of swelling agent (trimethylbenzene [TMB]) during the synthesis, the TiO_2 shell mesopores do not appear clearly after calcination in nitrogen. Through expanding the hydrophobic poly(propylene oxide) (PPO) chains of the composite micelles, the mesopore size of SL-mTiO_2 shells displays an increasing tendency from 4.9 to 17.8 nm observed from HRTEM results, in good accord with corresponding pore-size distribution curves (4.7–18.4 nm).

Moreover, we further demonstrated the versatility of this confined interfacial monomicelle assembly method by coating SL-mTiO_2 on a variety of nanomaterials, including carbon nanotubes (CNTs), graphene oxide (GO), carbon nanospheres,

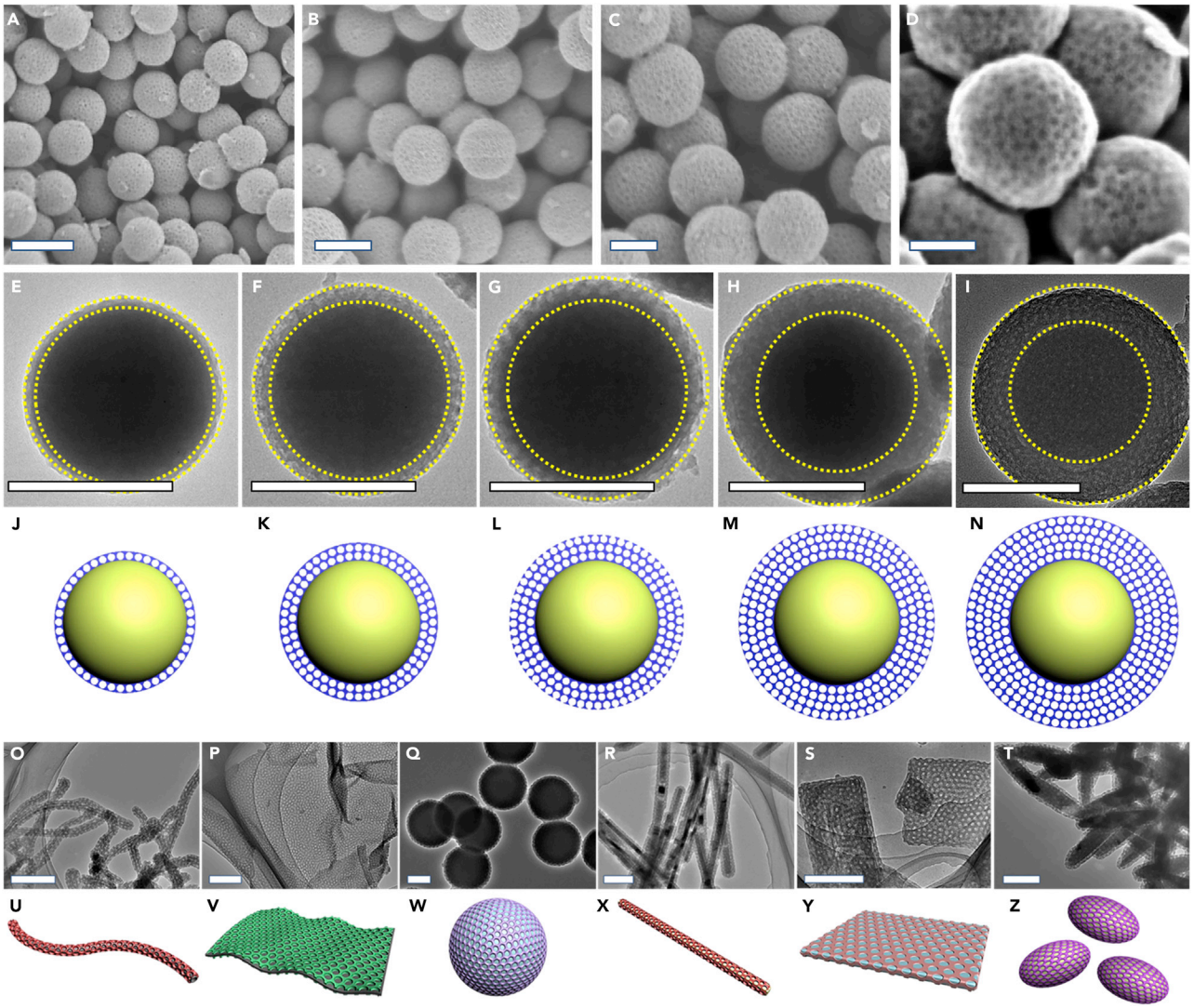

Figure 2. Precise Control of the Coated Mesoporous TiO_2 Layers

(A–D) SEM images of the core-shell SiO_2@SL-mTiO_2 nanospheres with varied silica core sizes at (A) 150, (B) 220, (C) 300, and (D) 420 nm.

(E–N) TEM images (E–I) and corresponding structural models (J–N) of the SiO_2@mTiO_2 core-shell structures with highly tunable coated TiO_2 layers from one to five layers of mesopores.

(O–Z) TEM images (O–T) and corresponding structural model (U–Z) of different nanomaterials from 1D to 3D with coated single-layered TiO_2 mesopores: (O) carbon nanotubes, (P) graphene oxides, (Q) carbon nanospheres, (R) CdS nanowires, (S) ZnS nanosheets, and (T) α-Fe_2O_3 ellipsoids. All scale bars represent 200 nm.

CdS nanowires, ZnS nanosheets, and α-Fe_2O_3 ellipsoids (Figures 2O–2Z and S17–S22). After calcination under nitrogen atmosphere, corresponding ordered TiO_2 mesopores can be formed uniformly on diverse surfaces, which possess strong interactions with hydroxyl groups for monomicelle heterogeneous growth. These results clearly suggest that SL-mTiO_2 shells enable coating on different functional nanomaterials with affiliations to micelles by using this universal method, which is independent of dimension, size, and composition of cores.

Electrochemical Properties of the Coated SL-mTiO_2

The electrochemical performances of the hollow SL-mTiO_2 nanospheres as a sodium-ion battery anode were investigated. As shown in current-voltage curves

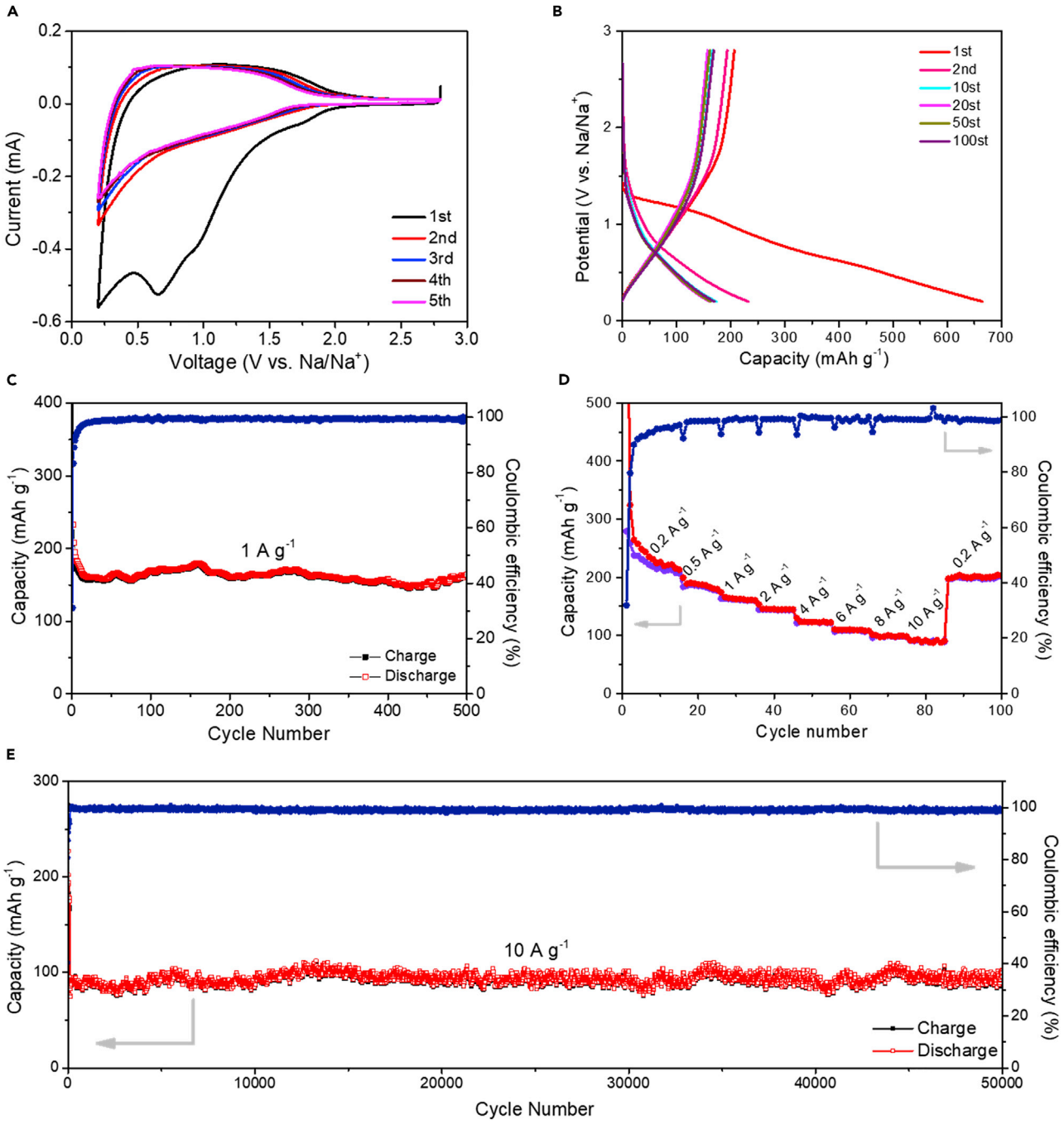

Figure 3. Electrochemical Properties of the Hollow SL-mTiO$_2$ Nanospheres as Na-Ion Battery

(A) Current-voltage curves of a sodium-ion battery at the initial five cycles.

(B) Charge-discharge profiles at the first, second, tenth, 20th, 50th, and 100th cycles under a current density of 1.0 A g^{-1}.

(C) Cycling stability and corresponding Coulombic efficiencies at a current density of 1.0 A g^{-1}.

(D) Charge-discharge capacities and corresponding Coulombic efficiencies at different current densities from 0.2 to 10.0 A g^{-1}.

(E) Long-term cycling performance at an ultrahigh current density of 10.0 A g^{-1}.

(Figure 3A), the cathodic peak at about 0.8 V can be attributed the formation of solid electrolyte interface films due to the reductive electrolyte decomposition.[35,36] *Ex situ* TEM and XRD analyses show the amorphous nature of the anode after initial

cycle, further suggesting the irreversible capacity loss during first cycle (Figure S23). The broad peak ranging from 0.5 to 1.0 V in the anodic scan is attributed to the Ti^{3+}/Ti^{4+} redox couple. The peak current density and integrated area intensity remain nearly constant from the third sweep process, indicating tiny capacity losses during cycling. The charge-discharge curves at 1.0 A g^{-1} present a high initial discharge of 665 mAh g^{-1} and charge capacity of 207 mAh g^{-1} (Figure 3B). Notably, the charge capacity undergoes a gradual decline over 1–20 cycles and a slight increment over 20–100 cycles, ascribed to the activation process and suppressed side reactions.[37] The capacity after 100 cycles still reaches 170 mAh g^{-1}, proving the high cyclability at a low rate. The Coulombic efficiency rises to nearly 95% in the tenth cycle, then reaches 99% in the 20th cycle and remains at this level for the subsequent cycles.

Meanwhile, the hollow SL-mTiO_2 nanospheres exhibit superior rate and cycling performances. Figure 3D shows the rate capacities of the sodium-ion battery, accompanied by the corresponding Coulombic efficiencies. The reversible capacities decrease slightly to 212 mAh g^{-1} at 0.2 A g^{-1} in the first 15 cycles. Thereafter, discharge capacities of 179, 160, 142, 122, 109, 97, and 89 mAh g^{-1} are achieved at 0.5, 1.0, 2.0, 4.0, 6.0, 8.0, and 10.0 A g^{-1}, respectively, and can almost return to 202 mAh g^{-1} when the current density resets to 0.2 A g^{-1}. Ultrahigh Coulombic efficiencies of nearly 99% are retained after 20 cycles over the whole test, suggesting excellent reversibility. Furthermore, we carried out long-term cycling stability measurements of the hollow SL-mTiO_2 nanospheres at both low and high rates. At a low current density of 1 A g^{-1}, the discharge capacity stabilizes at around 160 mAh g^{-1} after 20 cycles and remains at this level for over 500 cycles with high Coulombic efficiency of 99% (Figure 3C). Even at a high current density of 10 A g^{-1}, the capacity can still be retained at about 90 mAh g^{-1} for over 50,000 cycles (Figure 3E). Ninety-nine percent of the capacity is retained for each cycle, suggesting strong stability in ultralong cycles. By contrast, the hollow TiO_2 nanospheres and commercial P25 nanoparticles exhibit lower and less stable capacities at each specific current (Figure S24), with much lower capacities being retained at 1 A g^{-1} for these two electrodes (Figure S25). These results clearly demonstrate that the introduction of the interconnected mesoporosity can significantly enhance electrochemical properties due to the combination of electrolyte access and short diffusion lengths for both electronic and sodium-ion transport.

The impressive rate performance and outstanding cycling stability of the hollow SL-mTiO_2 nanospheres could be mainly attributed to the unique structural features, showing enhanced sodium-storage properties in comparison with reported TiO_2-based anode materials (Table S3). The mesoporous crystalline TiO_2 frameworks and hollow structures allow accommodation of volume expansion during sodium insertion-extraction. More importantly, the ultrathin TiO_2 mesostructures allow the entire high-surface-area mesoporous crystalline TiO_2 to comprehensively contact with electrolytes, thus facilitating rapid electrochemical reactions. Besides, the shortened diffusion lengths of sodium ions due to the single-layered mesopores also play an essential role for the highly reversible storage capacities. All of these structural features provide possibilities for achieving outstanding cycling and rate capabilities in sodium-ion storage.

DISCUSSION

Ex situ TEM measurements were conducted by harvesting products at different time intervals. After THF evaporation at 45°C for 24 h, the hydrogels of spherical

poly(ethylene oxide) (PEO)-PPO-PEO/TiO_2 oligomer composite monomicelles with a uniform diameter of ~12.4 nm are formed in high order (Figures S26 and S27), which is crucial for the subsequent confined assembly. Notably, TEM images display well-retained spherical morphology with declining regularity when dispersing the hydrogels in ethanol/glycerol solvents, implying that the Pluronic F127/TiO_2 monomicelles are surrounded by glycerol through hydrogen bonding (Figures S28A and S28B). It is worth mentioning that the glycerol-wrapped monomicelles turn out to be very stable, enabling prevention of monomicelle self-assembly at room temperature (Figures S28C and S29C). This phenomenon provides us the opportunity for precisely manipulating the assembly behavior. To further support this hypothesis we carried out the coating process at room temperature, which produced smooth silica spheres with no titania shells (Figures S29A and S29B). In contrast, when heating up to 100°C in the absence of silica cores, we observed the formation of white precipitates after the reaction (Figure S29D), confirming the strong monomicelle stability. As a result, we assumed that an external thermodynamic driving force is able to induce the assembly behavior of glycerol-stabilized monomicelles: If the collision between two monomicelles occurs under mild stirring, the surrounding glycerol is linked in advance. The glycerol in the middle region then moves away due to the mechanically unstable state[38,39] at a relatively high temperature, allowing the true connection and continuous condensation of the micellar dimers (Figure S29E).

Syntheses were also conducted by replacing glycerol and removing SiO_2 template for further investigation (Figures S30A–S30F). Nonuniform mesoporous TiO_2 spheres in different particle sizes appear after the reaction at 100°C when no co-solvent or other interactive solvents are added. Comparably, a heterogeneous nucleation and growth of the monomicelles occurred when using glycerol, evidenced from the 2D mesoporous TiO_2 nanosheets observed from SEM and TEM images (Figure S31). In consequence, the glycerol is proposed to perform as a special structure-directing and confined agent for TiO_2 monomicelle assembly. To validate this assumption, we measured the viscosities of these solvents at varying temperature. As expected, the viscosity of glycerol at room temperature is two orders of magnitude higher than in other solvents with hydroxyl groups (Figures S30G and S30H). It also appears to be five times as high as others even at 100°C, demonstrating its intrinsic viscous nature. This glycerol particularity is further validated by a controlled experiment in which no glycerol is added during the coating reaction (Figure S32). Thus we concluded that the strong hydrogen-bonding interaction provided by its three hydroxyl groups in one molecule, in combination with the ultrahigh viscosity, leads to glycerol being realized as a special protector and confined solvent of TiO_2 monomicelles.

Furthermore, we conducted controlled experiments in which the stirring rates were varied with or without colloidal silica template (Figure S33). The TEM results reveal well-retained SiO_2@SL-mTiO_2 core-shell structures or 2D mesoporous TiO_2 morphology under mild stirring at 350 rpm. However, when the stirring rate increases the mesoporous TiO_2 shells appear to be nonuniform and the uniform TiO_2 nanosheets become increasingly irregular at higher stirring rates. Thus, we considered that the relatively stronger shear force might interfere with the thermal motion of the confined monomicelles, leading to undesirably fast heterogeneous growth. On the other hand, we found that during the assembly process, the SL-mTiO_2 layers can be coated completely on the silica surface within 3 h and the core-shell mesostructure remains unchanged when the reaction time is prolonged to 24 h, showing that the reaction time has little impact on the coated mesostructure (Figures 4 and S34).

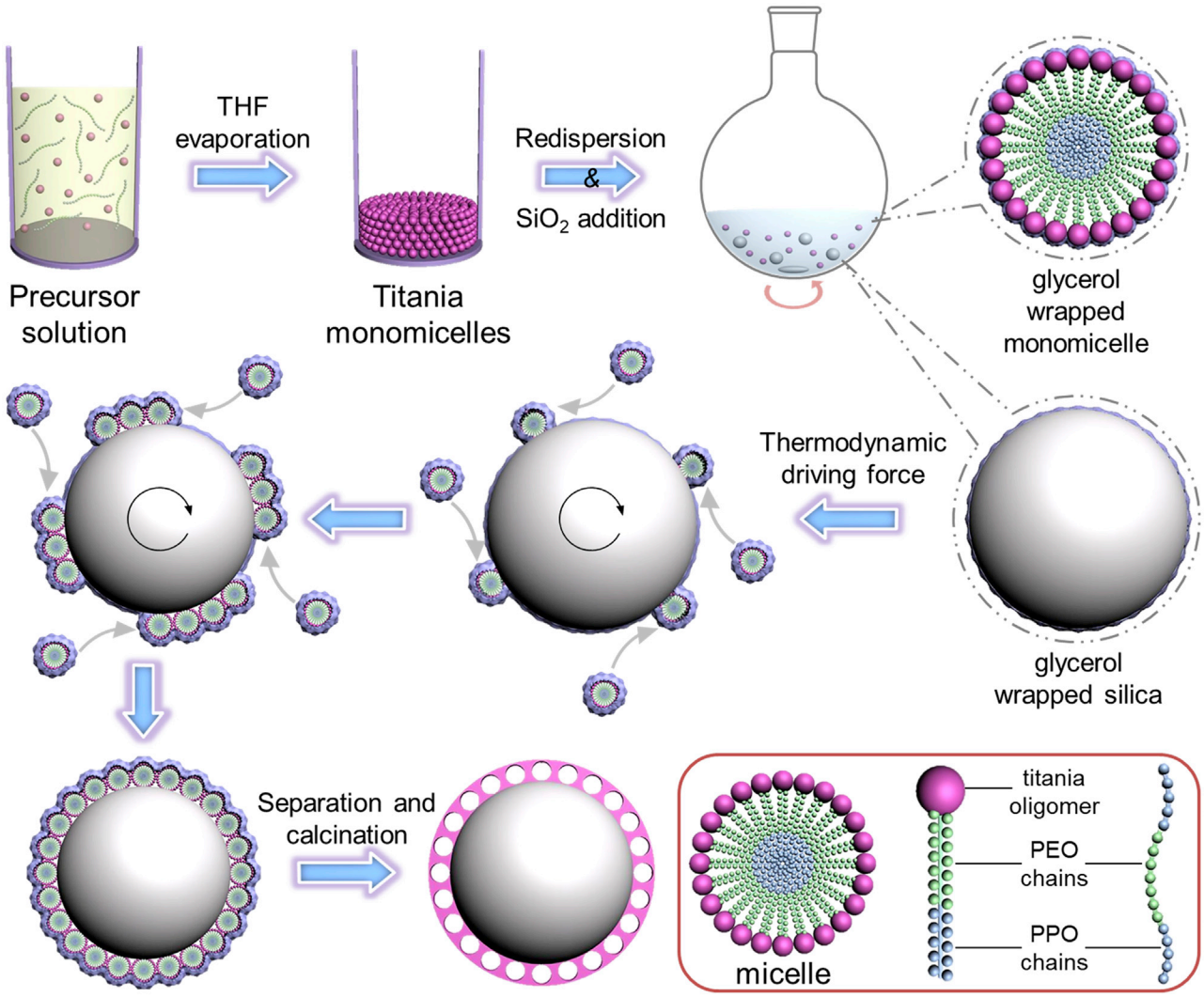

Figure 4. Schematic Illustration of the Formation Mechanism for Coating Single-Layered Mesoporous Titania via Confined Interfacial Monomicelle Assembly

On the basis of these observations, we propose a solvent-confined interfacial monomicelle self-assembly process for the controlled coating single-layered mesoporous TiO_2 on versatile solid surfaces. Before the growth of mesoporous TiO_2 shells, TBOT precursors hydrolyze slowly and assemble with hydrophilic PEO chains of Pluronic triblock copolymer F127; thus the uniform spherical PEO-PPO-PEO/TiO_2 oligomer composite monomicelles as coating subunits are formed previously by entire preferential THF evaporation at 45°C (as confirmed by *ex situ* TEM images). After redispersing in ethanol/glycerol mixture solution and introducing silica cores, the composite monomicelles and SiO_2 nanospheres are forced to be wrapped by glycerol solvent due to the strong hydrogen interaction provided by its three hydroxyl groups. A few F127/TiO_2 composite monomicelles start to collide and attach on large silica nanospheres under a mild shear force. When heating to 100°C, the surrounded glycerol becomes mechanically unstable, and thereby titania oligomers and silica nanospheres are able to link together after heat flow of the glycerol molecular networks in between. The titania monomicelles then prefer to pack side by side on the silica surface with continuous glycerol thermal flow because of the much

stronger interaction at solid-liquid interface. Due to the confinement effect of surrounding glycerol solvent networks, the assembly on the monomicelle surface away from silica cores is much unfavored. After continuous collision and assembly at the silica solid surface, single-layer close-packed SiO_2@TiO_2 nanospheres with ordered mesostructure are formed. The uniform SiO_2@SL-mTiO_2 nanospheres are finally obtained after crystallization and surfactant removal by annealing in an inert atmosphere. Furthermore, if the glycerol/TiO_2 monomicelle ratio or SiO_2/TiO_2 monomicelle ratio decrease, the confinement effect is weakened. The continuous assembly is gradually favored, leading to the growth of multilayered mesopores.

Conclusion

In summary, we have demonstrated a novel confined interfacial monomicelle assembly approach for the growth of single-layered crystalline TiO_2 mesopores on diverse interfaces (SiO_2, carbon, polymers, metal oxides, metal sulfides). Controlled growth of uniform mesoporous TiO_2 shells with a tunable number of the coated layers, mesopore size, and switchable coated surfaces have been achieved. Such successful precision synthesis requires the preformation of TiO_2 monomicelle hydrogels and the solvent-confinement effect of glycerol. The formed SL-mTiO_2 shells have shown excellent rate capability and superior cyclability as a sodium-ion battery anode. Moreover, this finding reveals the significance of the confinement effect in the controlled synthesis of well-defined nanostructures. Such accurately designed core-shell nanostructures also provide a solid platform for the construction of multicomponent nanostructures with diverse functionalities, which might have great potential for practical applications.

EXPERIMENTAL PROCEDURES

Preparation of Spherical PEO-PPO-PEO/TiO_2 Oligomer Composite Monomicelle Gels

The gels of PEO-PPO-PEO/TiO_2 oligomer composite monomicelles were synthesized according to an evaporation-driven oriented assembly approach.[40] For a typical synthesis, 1.5 g of triblock copolymer Pluronic F127, 2.4 mL of acetic acid, and 3.2 mL of concentrated HCl were added stepwise into 30.0 mL of THF, then 3.0 mL of TBOT was added dropwise into the mixture to form a golden-yellow solution. After vigorous stirring for 10 min, the white-yellow solution (around 40 mL in total) was transferred into two 30 × 50-mm volumetric flasks and kept in an oven at 45°C for 24 h to slowly evaporate THF solvent. The white-yellow gels of spherical F127/TiO_2 composite monomicelles were obtained and stored in a drying box.

Fabrication of SiO_2@SL-mTiO_2 Core-Shell Nanostructures

In brief, the coating of single-layered TiO_2 mesopores on the colloidal silica nanospheres was carried out via an improved hydrothermal-induced solvent-confined monomicelle assembly method.[33] In a typical process, 3.0 g of above-formed gels and 3.0 mL of TMB were redispersed in 10.0 mL of anhydrous ethanol under stirring for 10 min. Glycerol (10.0 mL) was subsequently added dropwise. After stirring for 5 min to form a transparent solution, 2.0 mL of anhydrous ethanol containing 1.0 g of monodispersed SiO_2 nanospheres (~220 nm) obtained as above were added into the mixture. The whole solution was heated in an oil bath at 100°C for 6 h under mild stirring (350 rpm) and allowed to cool down to room temperature. The white precipitates were isolated and collected by centrifugation, washed with ethanol, and dried in an oven. Finally the SiO_2@SL-mTiO_2 core-shell structures were obtained after annealing under nitrogen at 350°C for 3 h to remove F127 template and improve crystallinity. The nitrogen atmosphere was used to prevent mesostructural collapse during annealing. The hollow mesoporous TiO_2 nanospheres

were formed by etching silica cores with NaOH solution (2.0 M) at 80°C for 24 h. The syntheses of SiO_2@mTiO_2 core-shell structures with various diameters were performed through same processes except for adding the SiO_2 cores with diameters at 150, 300, and 420 nm, respectively. The syntheses of SiO_2@mTiO_2 core-shell structures with different layers of mesopores were performed through same processes except for varying the glycerol amount to 7.5, 5.5, 4.0, and 3.0 mL, or changing the SiO_2 amount to 0.50, 0.25, 0.12, and 0.08 g, respectively.

Fabrication of SL-mTiO_2-Coated Core-Shell Structures with Diverse Core Particles

In brief, the SL-mTiO_2-coated core-shell structures were prepared under the same conditions as for coating silica nanospheres except for replacing the SiO_2 cores with 50 mg of GOs, 50 mg of CNTs, 0.8 g of carbon nanospheres, 1.5 g of CdS nanowires, 1.5 g of CdS nanorods, 2.0 g of ZnS nanosheets, and 1.0 g of α-Fe_2O_3 ellipsoids, respectively. Of note, the coating processes for α-Fe_2O_3 ellipsoids were carried out with a magnetic stirrer.

SUPPLEMENTAL INFORMATION

Supplemental Information can be found online at https://doi.org/10.1016/j.matt.2019.03.003.

ACKNOWLEDGMENTS

This work is supported by the State Key Basic Research Program of China (2017YFA0207303), the National Natural Science Foundation of China (21733003), the Shanghai Leading Academic Discipline Project (B108), and the Science and Technology Commission of Shanghai Municipality (17JC1400100). K.L. acknowledges the financial support by the China Scholarship Council (201806100112). A.E. acknowledges Qatar University under GCC Co-Fund Program grant GCC-2017-001.

AUTHOR CONTRIBUTIONS

Conceptualization, K.L. and D.Z.; Methodology, K.L. and D.Z.; Investigation, K.L., Y.X., R.W., Z.Z., W.Z., X.Z., and A.E.; Writing – Original Draft, K.L. and D.Z.; Writing – Review and Editing, K.L. and D.Z.; Supervision, D.Z.; Funding Acquisition, D.Z. and A.E.

DECLARATION OF INTERESTS

The authors declare no competing interests.

Received: January 5, 2019
Revised: February 23, 2019
Accepted: March 13, 2019
Published: May 15, 2019

REFERENCES

1. Chaudhuri, R.G., and Paria, S. (2012). Core/shell nanoparticles: classes, properties, synthesis mechanisms, characterization, and applications. Chem. Rev. *112*, 2373–2433.

2. Gawande, M.B., Goswami, A., Asefa, T., Guo, H.Z., Biradar, A.V., Peng, D.L., and Varma, R.S. (2015). Core-shell nanoparticles: synthesis and applications in catalysis and electrocatalysis. Chem. Soc. Rev. *44*, 7540–7590.

3. Lu, Y., Yin, Y., and Xia, Y. (2001). A self-assembly approach to the fabrication of patterned, two-dimensional arrays of microlenses of organic polymers. Adv. Mater. *13*, 271–274.

4. Yin, Y., Lu, Y., Sun, Y., and Xia, Y. (2002). Silver nanowires can be directly coated with amorphous silica to generate well-controlled coaxial nanocables of silver/silica. Nano Lett. *2*, 427–430.

5. Lauhon, L.J., Gudiksen, M.S., Wang, D.L., and Lieber, C.M. (2002). Epitaxial core-shell and core-multishell nanowire heterostructures. Nature *420*, 57–61.

6. Tian, B.Z., Zheng, X.L., Kempa, T.J., Fang, Y., Yu, N.F., Yu, G.H., Huang, J.L., and Lieber, C.M. (2007). Coaxial silicon nanowires as solar cells and nanoelectronics power sources. Nature *449*, 885–889.

7. Tang, J.Y., Huo, Z.Y., Brittman, S., Gao, H.W., and Yang, P.D. (2011). Solution-processed core-shell nanowires for efficient photovoltaic cells. Nat. Nano *6*, 568–572.

8. Li, X.M., Zhang, F., and Zhao, D.Y. (2015). Lab on upconversion nanoparticles: optical properties and applications engineering via designed nanostructure. Chem. Soc. Rev. *44*, 1346–1378.

9. Zhang, J.T., Tang, Y., Lee, K., and Ouyang, M. (2010). Nonepitaxial growth of hybrid core-shell nanostructures with large lattice mismatches. Science *327*, 1634–1638.

10. Yang, S.B., Feng, X.L., and Müllen, K. (2011). Sandwich-like, graphene-based titania nanosheets with high surface area for fast lithium storage. Adv. Mater. *23*, 3575–3579.

11. Zhu, G.N., Du, Y.J., Wang, Y.G., Yu, A.S., and Xia, Y.Y. (2013). Electrochemical profile of lithium titanate/hard carbon composite as anode material for Li-ion batteries. J. Electro. Chem. *688*, 86–92.

12. Wang, Z.Y., Zhou, L., and Lou, X.W. (2012). Metal oxide hollow nanostructures for lithium-ion batteries. Adv. Mater. *24*, 1903–1911.

13. Lai, X.Y., Halpert, J.E., and Wang, D. (2012). Recent advances in micro-/nano-structured hollow spheres for energy applications: from simple to complex systems. Energy Environ. Sci. *5*, 5604–5618.

14. El-Toni, A.M., Habila, M.A., Labis, J.P., Alothman, Z.A., Alhoshan, M., Elzatahry, A.A., and Zhang, F. (2016). Design, synthesis and applications of core-shell, hollow core, and nanorattle multifunctional nanostructures. Nanoscale *8*, 2510–2531.

15. Liu, J., Wickramaratne, N.P., Qiao, S.Z., and Jaroniec, M. (2015). Molecular-based design and emerging applications of nanoporous carbon spheres. Nat. Mater. *14*, 763–774.

16. Li, W., Liu, J., and Zhao, D.Y. (2016). Mesoporous materials for energy conversion and storage devices. Nat. Rev. Mater. 16023, https://doi.org/10.1038/natrevmats.2016.23.

17. Joo, J.B., Lee, I., Dahl, M., Moon, G.D., Zaera, F., and Yin, Y. (2013). Controllable synthesis of mesoporous TiO_2 hollow shells: toward an efficient photocatalyst. Adv. Funct. Mater. *23*, 4246–4254.

18. Joo, J.B., Dahl, M., Li, N., Zaera, F., and Yin, Y. (2013). Tailored synthesis of mesoporous TiO_2 hollow nanostructures for catalytic applications. Energy Environ. Sci. *6*, 2082–2092.

19. Fang, Y., Lv, Y.Y., Gong, F., Elzatahry, A.A., Zheng, G.F., and Zhao, D.Y. (2016). Synthesis of 2D-mesoporous-carbon/MoS_2 heterostructures with well-defined interfaces for high- performance lithium-ion batteries. Adv. Mater. *28*, 9385–9390.

20. Deng, Y.H., Qi, D.W., Deng, C.H., Zhang, X.M., and Zhao, D.Y. (2008). Superpara-magnetic high-magnetization microspheres with an Fe_3O_4@SiO_2 core and perpendicularly aligned mesoporous SiO_2 shell for removal of microcystins. J. Am. Chem. Soc. *130*, 28–29.

21. Li, X.M., Zhou, L., Wei, Y., El-Toni, A.M., Zhang, F., and Zhao, D.Y. (2015). Anisotropic encapsulation-induced synthesis of asymmetric single-hole mesoporous nanocages. J. Am. Chem. Soc. *137*, 5903–5906.

22. Teng, Z.G., Su, X.D., Lee, B.H., Huang, C.G., Liu, Y., Wang, S.J., Wu, J., Xu, P., Sun, J., Shen, D.G., et al. (2014). Yolk-shell structured mesoporous nanoparticles with thioether-bridged organosilica frameworks. Chem. Mater. *26*, 5980–5987.

23. Teng, Z.G., Wang, S., Su, X., Chen, G., Liu, Y., Luo, Z., Luo, W., Tang, Y., Ju, H., Zhao, D., and Lu, G. (2014). Facile synthesis of yolk-shell structured inorganic-organic hybrid spheres with ordered radial mesochannels. Adv. Mater. *26*, 3741–3747.

24. Yue, Q., Li, J., Zhang, Y., Cheng, X., Chen, X., Pan, P., Su, J., Elzatahry, A.A., Alghamdi, A., Deng, Y., and Zhao, D. (2017). Plasmolysis-inspired nanoengineering of functional yolk-shell microspheres with magnetic core and mesoporous silica shell. J. Am. Chem. Soc. *139*, 15486–15493.

25. Hu, Y., Gao, X.H., Yu, L., Wang, Y.R., Ning, J.Q., Xu, S.J., and Lou, X.W. (2013). Carbon-coated CdS petalous nanostructures with enhanced photostability and photocatalytic activity. Angew. Chem. Int. Ed. *52*, 5636–5639.

26. Guan, B.Y., Yu, L., and Lou, X.W. (2016). Chemically assisted formation of monolayer colloidsomes on functional particles. Adv. Mater. *28*, 9596–9601.

27. Pierre, A.C., and Pajonk, G.M. (2002). Chemistry of aerogels and their applications. Chem. Rev. *102*, 4243–4265.

28. Li, W., Yang, J.P., Wu, Z.X., Wang, J.X., Li, B., Feng, S.S., Deng, Y.H., Zhang, F., and Zhao, D.Y. (2012). A versatile kinetics-controlled coating method to construct uniform porous TiO_2 shells for multifunctional core-shell structures. J. Am. Chem. Soc. *134*, 11864–11867.

29. Guan, B.Y., Yu, L., Li, J., and Lou, X.W. (2016). A universal cooperative assembly-directed method for coating of mesoporous TiO_2 nanoshells with enhanced lithium storage properties. Sci. Adv. *2*, e1501554.

30. Joo, J.B., Zhang, Q., Lee, I., Dahl, M., Zaera, F., and Yin, Y. (2012). Mesoporous anatase titania hollow nanostructures though silica-protected calcination. Adv. Funct. Mater. *22*, 166–174.

31. Detavernier, C., Dendooven, J., Sree, S.P., Ludwig, K.F., and Martens, J.A. (2011). Tailoring nanoporous materials by atomic layer deposition. Chem. Soc. Rev. *40*, 5242–5253.

32. Liu, R., and Sen, A. (2012). Controlled synthesis of heterogeneous metal-titania nanostructures and their applications. J. Am. Chem. Soc. *134*, 17505–17512.

33. Lan, K., Liu, Y., Zhang, W., Liu, Y., Elzatahry, A., Wang, R.C., Xia, Y.Y., Al-Dhayan, D., Zheng, N.F., and Zhao, D.Y. (2018). Uniform ordered two-dimensional mesoporous TiO_2 nanosheets from hydrothermal-induced solvent-confined monomicelle assembly. J. Am. Chem. Soc. *140*, 4135–4143.

34. Li, F., Wang, Z.Y., Ergang, N.S., Fyfe, C.A., and Stein, A. (2007). Controlling the shape and alignment of mesopores by confinement in colloidal crystals: designer pathways to silica monoliths with hierarchical porosity. Langmuir *23*, 3996–4004.

35. Ye, C., Zhang, L., Guo, C.X., Li, D.D., Vasileff, A., Wang, H.H., and Qiao, S.Z. (2017). A 3D hybrid of chemically coupled nickel sulfide and hollow carbon spheres for high performance lithium-sulfur batteries. Adv. Funct. Mater. *27*, 1702524.

36. Wu, L.M., Bresser, D., Buchholz, D., Griffin, G.A., Castro, C.R., Ochel, A., and Passerini, S. (2015). Unfolding the mechanism of sodium insertion in anatase TiO_2 nanoparticles. Adv. Energy Mater. *5*, 1401142.

37. Xie, F.X., Zhang, L., Su, D.W., Jaroniec, M., and Qiao, S.Z. (2017). $Na_2Ti_3O_7$@N-doped carbon hollow spheres for sodium-ion batteries with excellent rate performance. Adv. Mater. *29*, 1700989.

38. Furukawa, A., and Tanaka, H. (2006). Violation of the incompressibility of liquid by simple shear flow. Nature *443*, 434–438.

39. Vutukuri, H.R., Bet, B., Roij, R.V., Dijkstra, M., and Huck, W.T.S. (2017). Rational design and dynamics of self-propelled colloidal bead chains: from rotators to flagella. Sci. Rep. *7*, 16758.

40. Liu, Y., Che, R., Chen, G., Fan, J., Sun, Z., Wu, Z., Wang, M., Li, B., Wei, J., Wei, Y., et al. (2015). Radially oriented mesoporous TiO_2 microspheres with single-crystal-like anatase walls for high-efficiency optoelectronic devices. Sci. Adv. *1*, e1500166.